星形成ゼミ

SFN #301 (15-21本目)

百瀬宗武（茨城大・理）

ハイライトは以下の３本（特に最後の）

- #16: Robo-AO Discovery and Basic Characterization of Wide Multiple Star Systems in the Pleiades, Praesepe, and NGC 2264 Clusters (Hillenbrand et al. AJ, 155:51 (15pp))
- #18: A search for pre- and proto-brown dwarfs in the dark cloud Barnard 30 with ALMA (Huélamo et al., A&A 597, A17)
- #19: The ALMA-PILS survey: 3D modeling of the envelope, disks and dust filament of IRAS 16293–2422 (Jacobsen et al. A&A in press)

16. Robo-AO Discovery and Basic Characterization of Wide Multiple Star Systems in the Pleiades, Praesepe, and NGC 2264 Clusters

L. Hillenbrand et al. (AJ, 155, 51)

http://ads.nao.ac.jp/abs/2018AJ....155...51H

【背景】(1) バイナリーの頻度分布については，様々な依存性が議論されている（Field stars vs. YSO clusters や Open clusters；中心星質量依存性など）。(2) 装置面では，小口径用望遠鏡に開発されたフルオートの laser ガイド付き Robo-AOを開発，多天体サーベイに威力発揮。

【研究内容】パロマー60インチ(1.5m)望遠鏡 + Robo-AOを組み合わせ，Pleiades, Praescepe, NGC2264の全構成メンバーの約10%（J等級=10-13.5）について，波長600nmイメージングによるbinary探査を実施。

	距離	年齢	構成メンバー数	今回の観測ターゲット	バイナリー検出※	対象のSp. Type
Pleiades	136±1 pc	125±8 Myr	~1500	212	32	K & early M
Praescepe	179±2 pc	757±36 Myr	~1000	108	8	K & early M
NGC 2264	740pc あるいは 913pc	~ 3Myr	~1500	120	34	FGK (YSOs)

※ 以前から知られていたのは10%のみ

・イメージングの実際

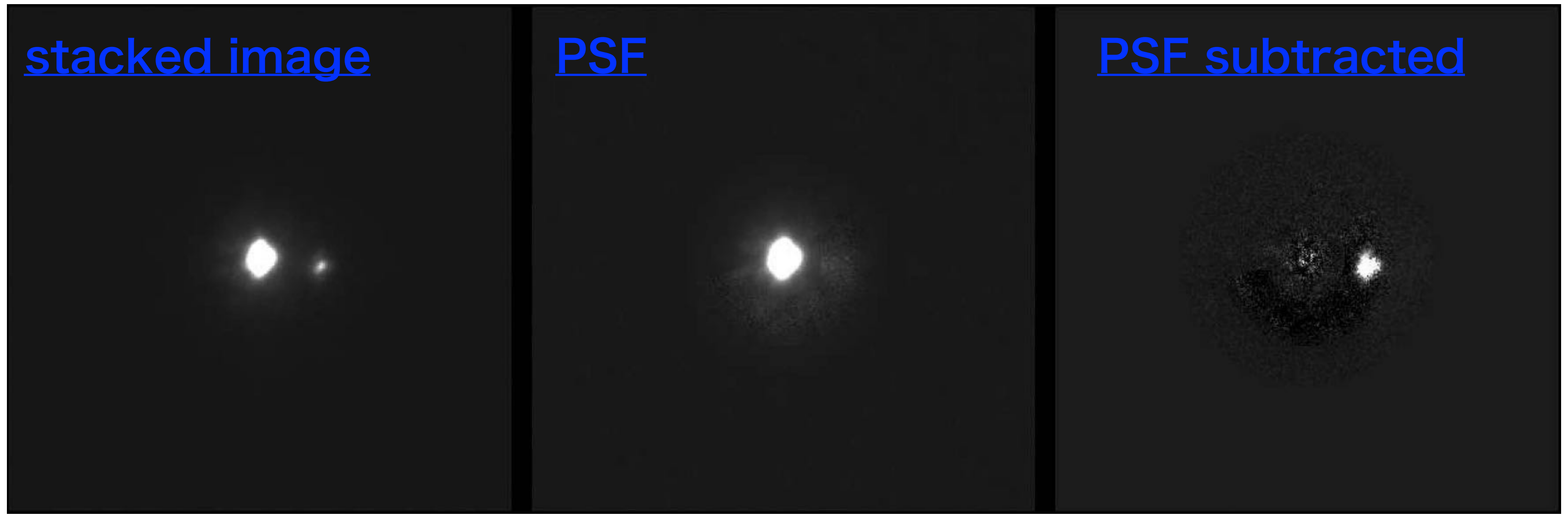

Figure 1. Shown here are the stacked image cutout (left), the PSF image assembled from images surrounding the leftmost image in time (center), and the PSF-subtracted remainder image (right) that isolates the secondary star for AK IV-314, a binary system having separation 1$''$.0. North is up and east is to the right.

・コントラストカーブの例

(左) stacked image上
(右) PSF差引後

※ 0.2” = 2λ/D 以内の伴星検出は不可能

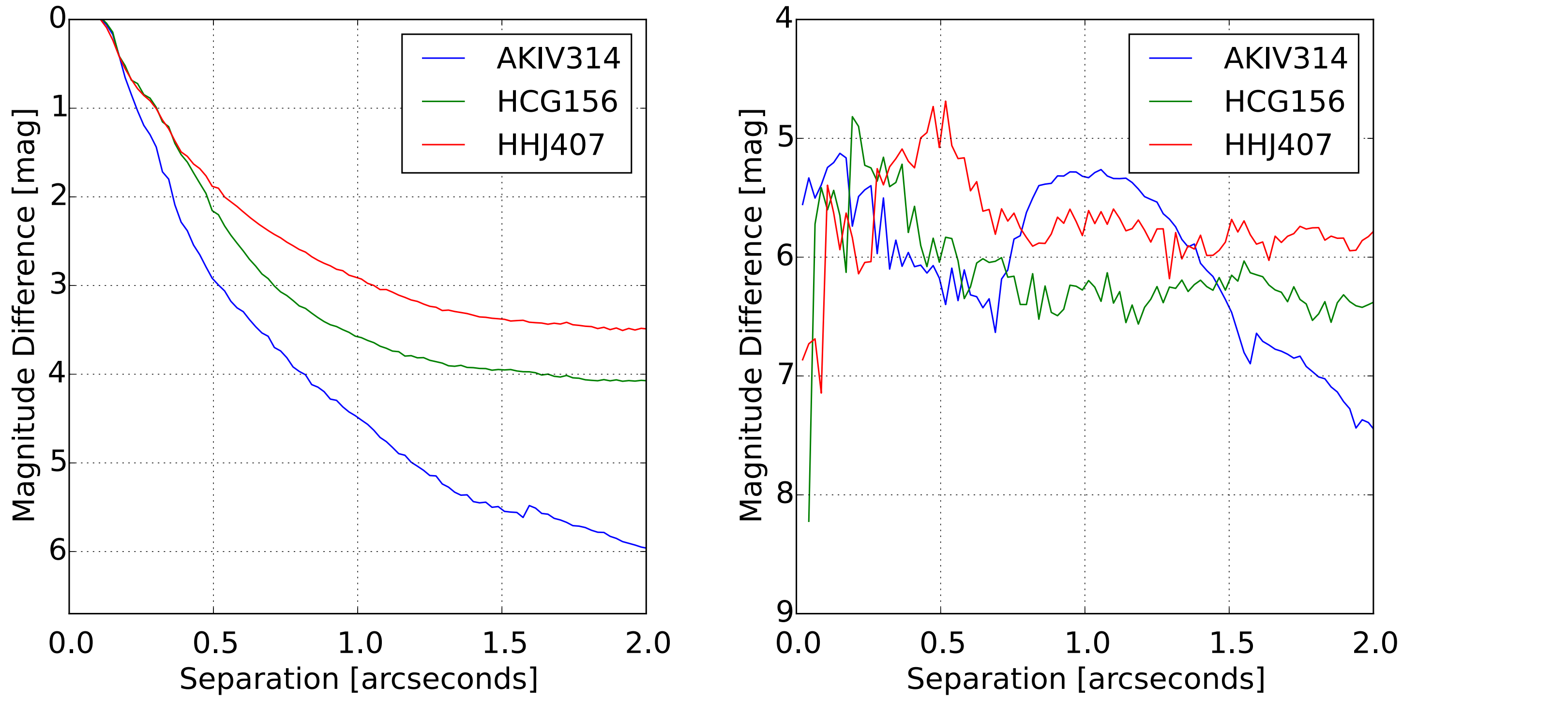

Figure 5. Contrast curves for three stars of varying image quality; raw contrast is on the left and PSF-subtracted contrast on the right. The stars illustrated are: AK IV-314, which was one of the most well-imaged stars, but is a binary system with separation of 1$''$.03; the secondary has been subtracted before generating the contrast curves (resulting in the artifact discontinuity around 1$''$.6). HCG-156 is representative of the mean performance, and is a single star. HHJ-407 is about one standard deviation away from the mean performance. As illustrated in the right panel, PSF subtraction improves the contrast by several magnitudes, though companion detection is still not possible below ~0$''$.2 (roughly 2 × λ/D). The broad bump for AK IV-314 is the residual of the seeing halo of the subtracted companion.

・separation vs. ΔMag

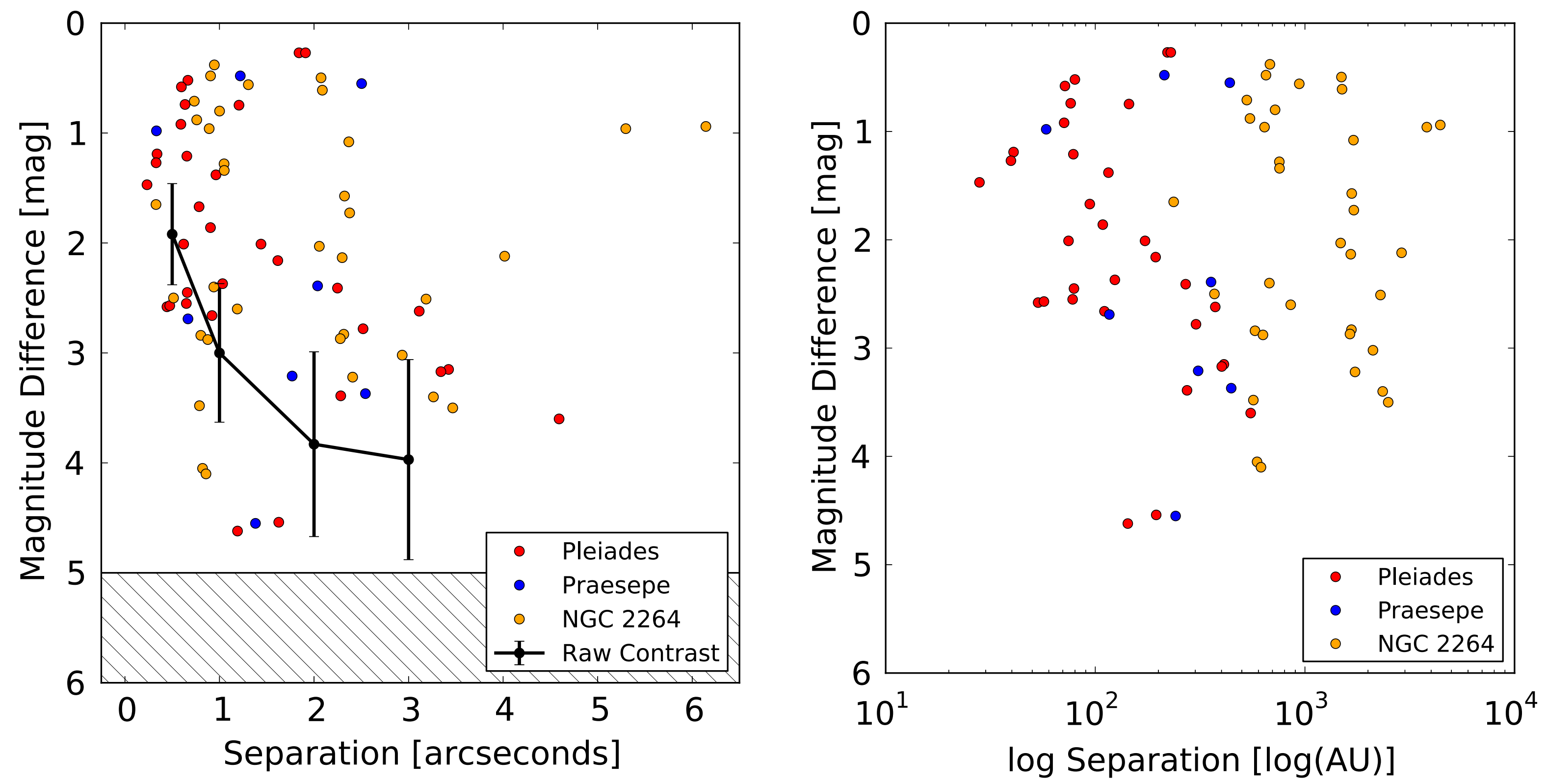

プレアデス

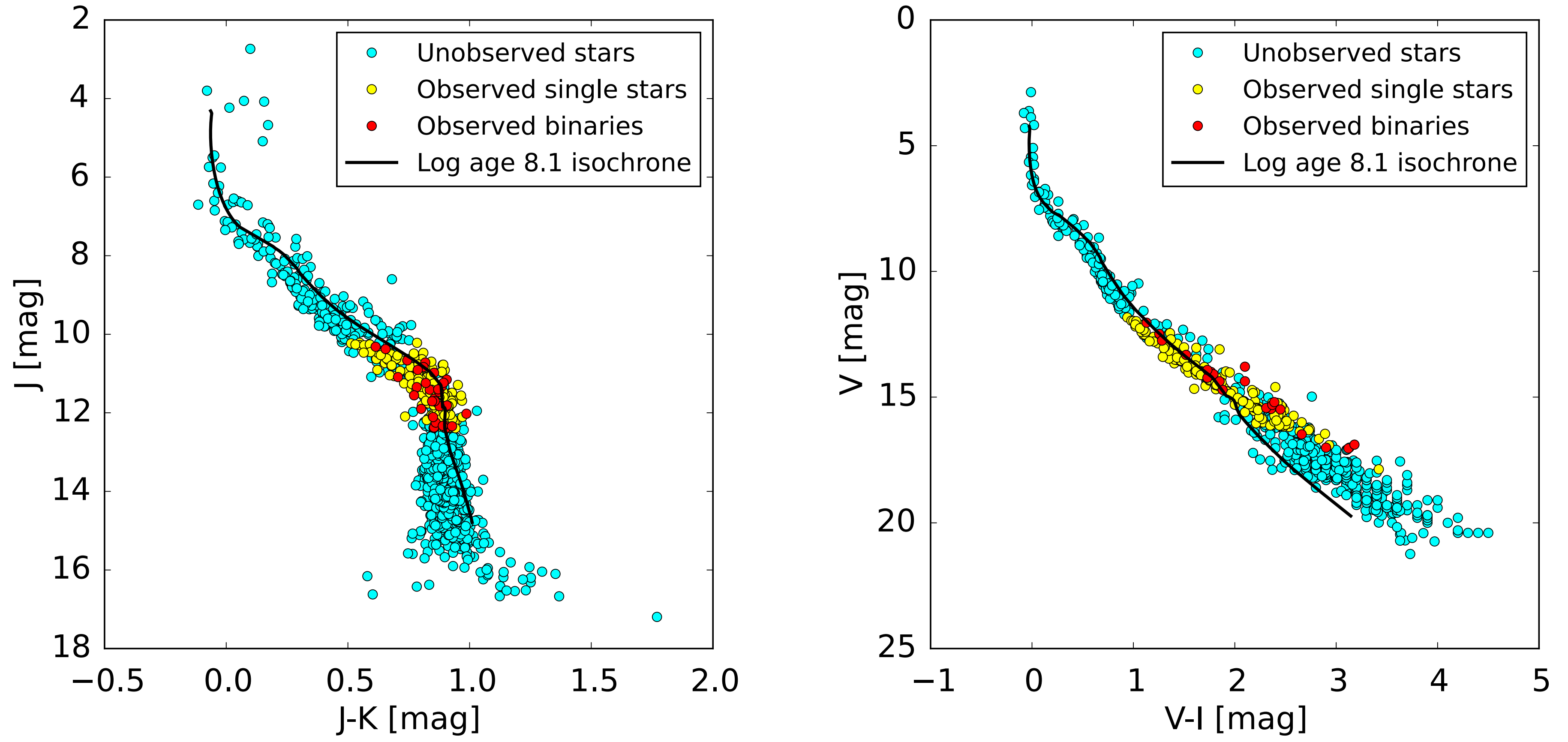

プレセペ

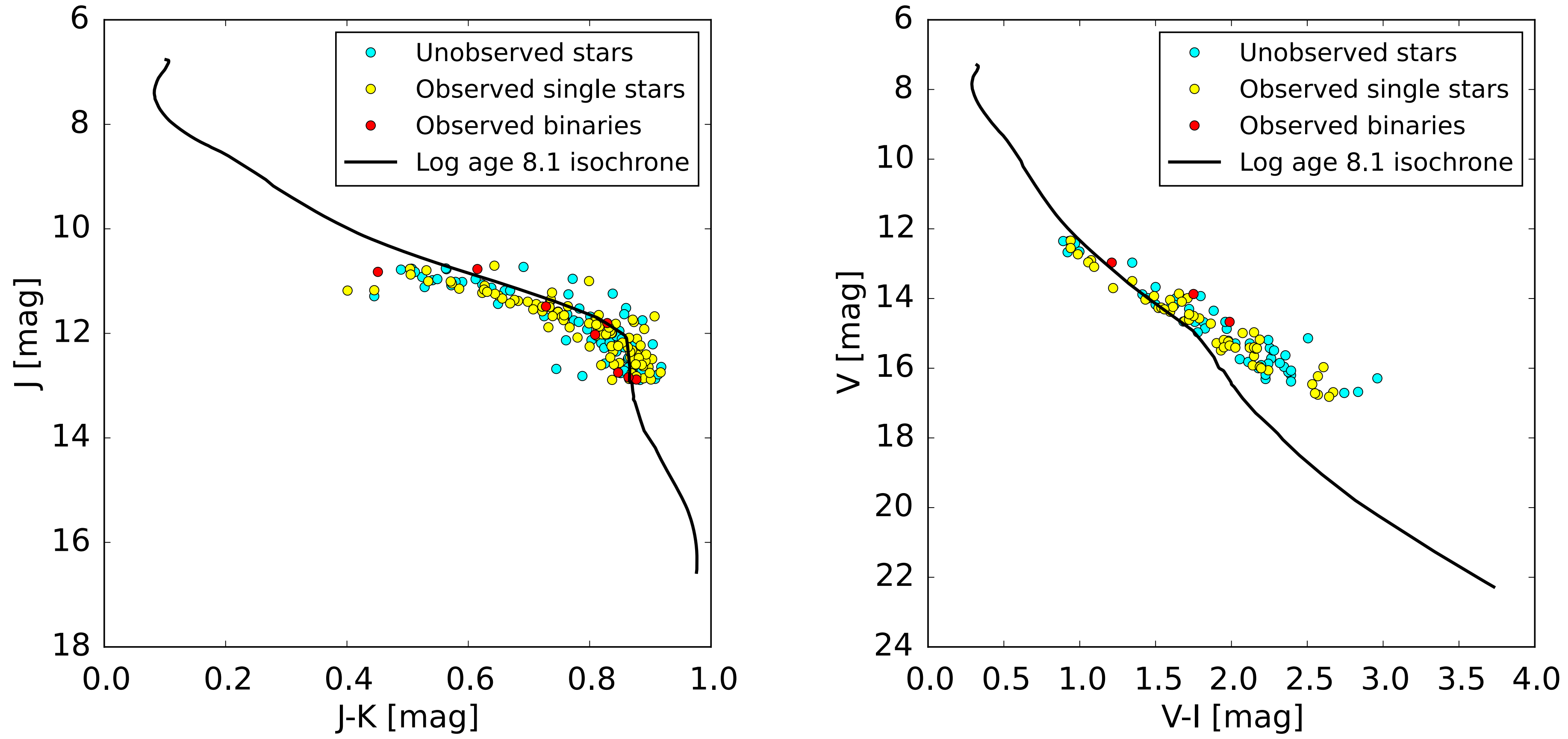

NGC 2264

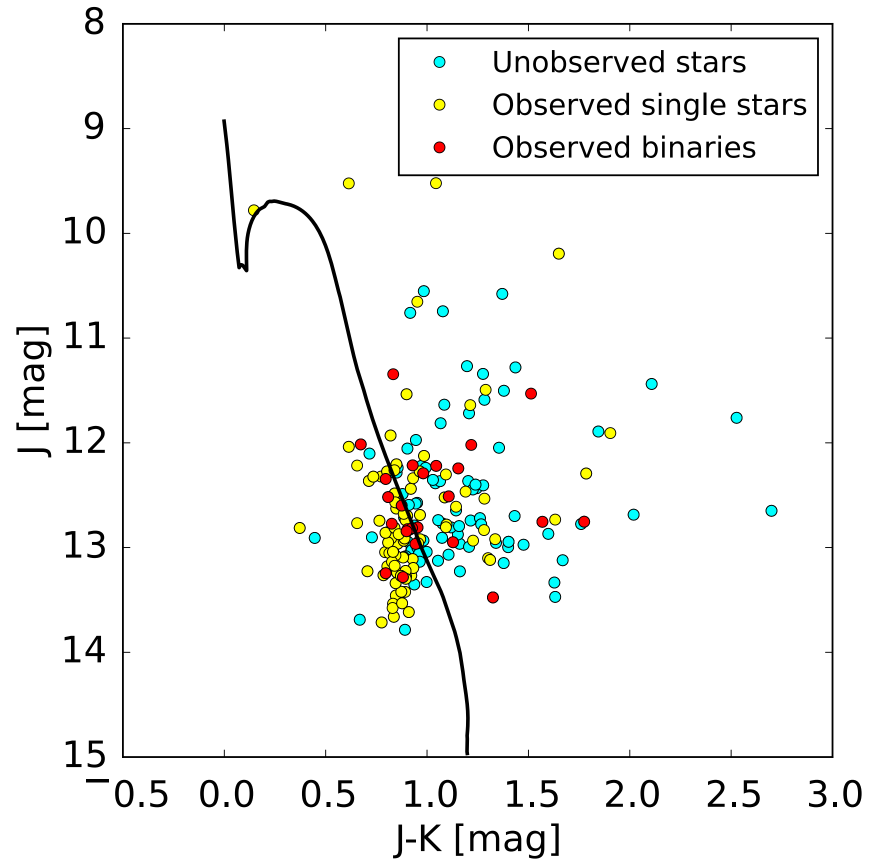

- 水色：観測しなかった天体
- 黄色：観測，単独星
- 赤色：観測，バイナリー
- 黒線はisochrone 理論モデルから期待される色等級図のライン

- プレアデスとプレセペの質量比分布

※0.2-0.9の範囲に分布

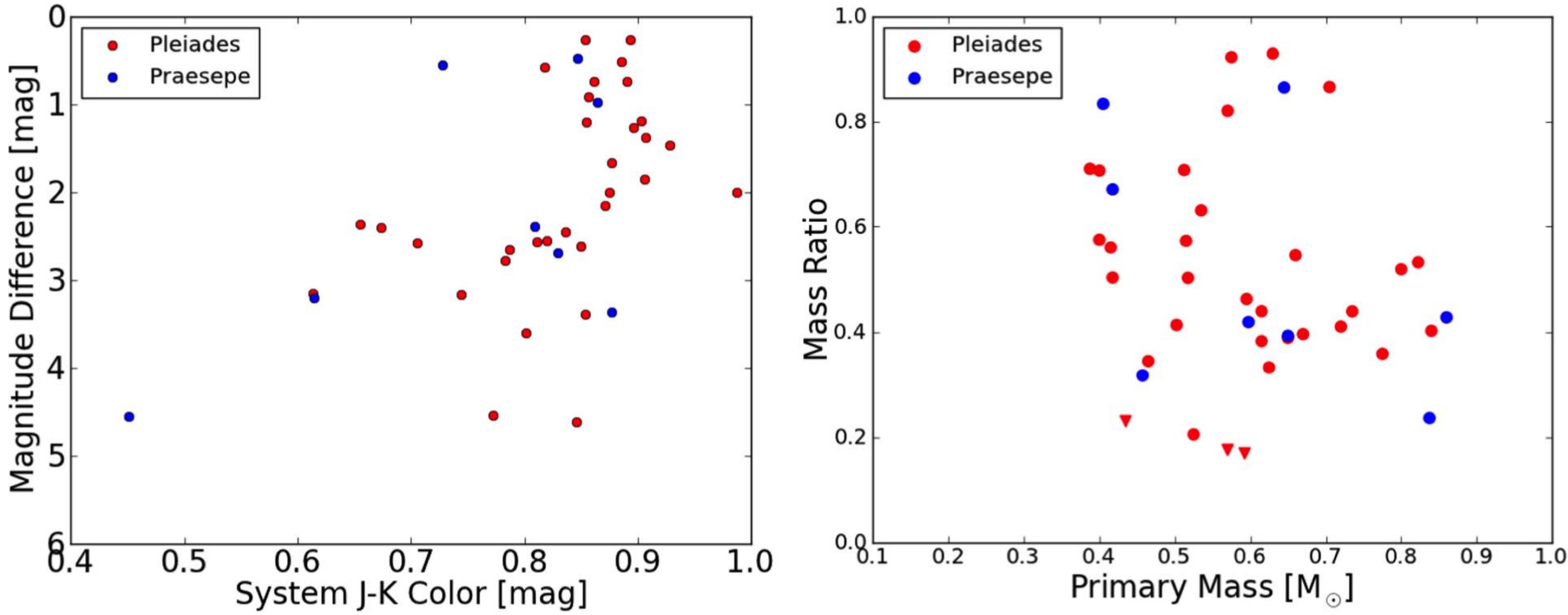

Figure 10. Magnitude difference as a function of system composite color (left) and corresponding inferred mass ratio as a function of primary mass (right) for the Pleiades (red, with upper limits indicated by inverted triangles set by the lowest masses available from the adopted evolutionary tracks) and Praesepe (blue) binary samples. As the distributions are dominated by small-number statistics, no conclusions can be drawn beyond illustration of the range in q of the detected binaries.

全体としての Binary 検出率は

15.5 ± 2 %

18. A search for pre- and proto-brown dwarfs in the dark cloud Barnard 30 with ALMA

S. K. Huélamo et al., A&A 597, A17

http://ads.nao.ac.jp/abs/2017A%26A...597A..17H

【目的・内容】褐色矮星の起源を探る一環として，Lambda Orionis 中にある暗黒星雲 B30中のコアの小質量側を探査。APEX/LABOCA の870μm ダスト連続波広域マップをもとに同定された30のコアを，ALMA 880μm で観測（Cycle 1）。APEX/SABOCA 350μmデータも補助的に使用。

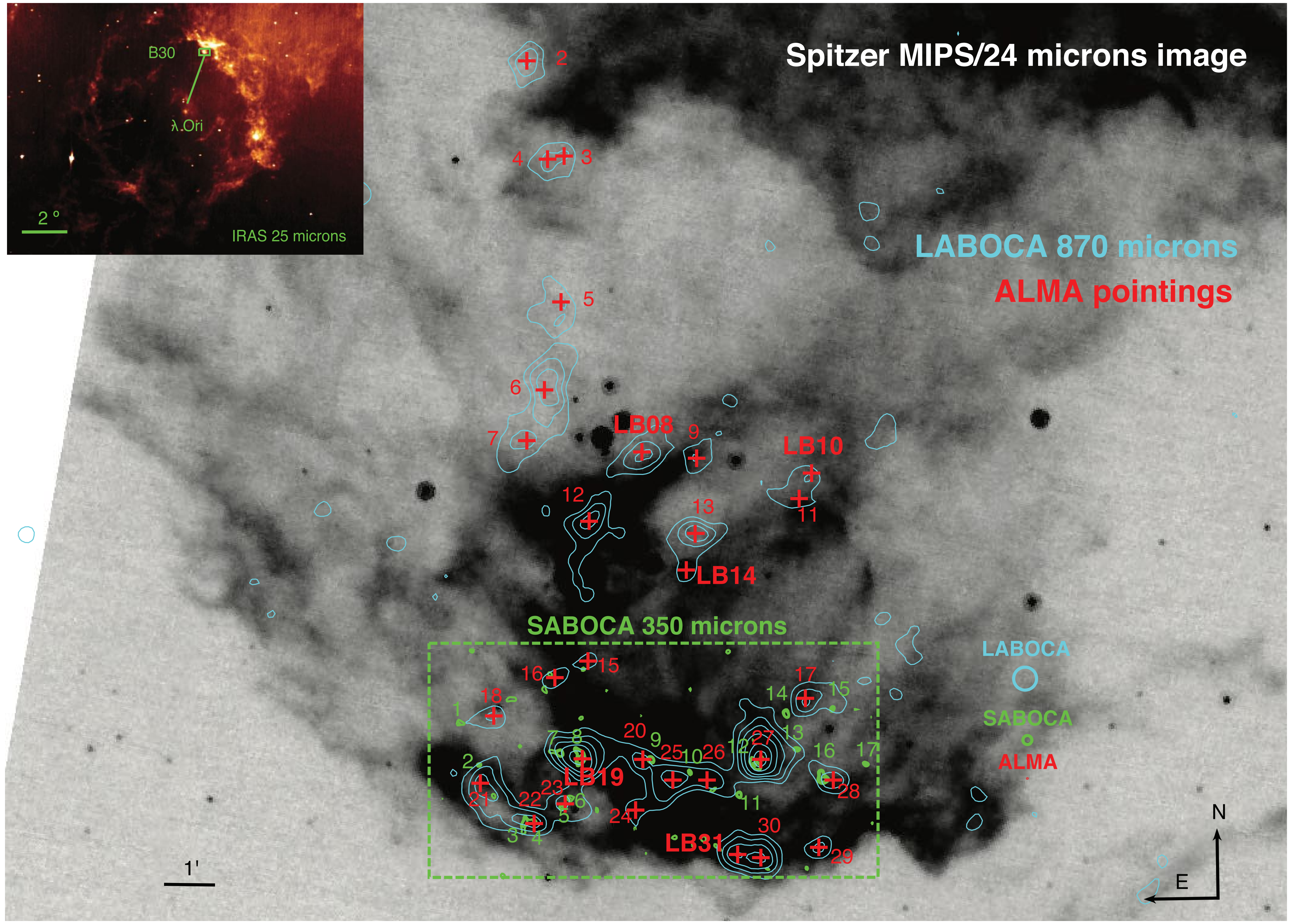

【観測・解析】

- Baseline = (15-395) kλ,　0.95” x 0.50”,　検出できる最大サイズ ~ 6”
- 30のコア中ALMAの検出は5個(Fig 1),　全てλOri の電離領域中に存在

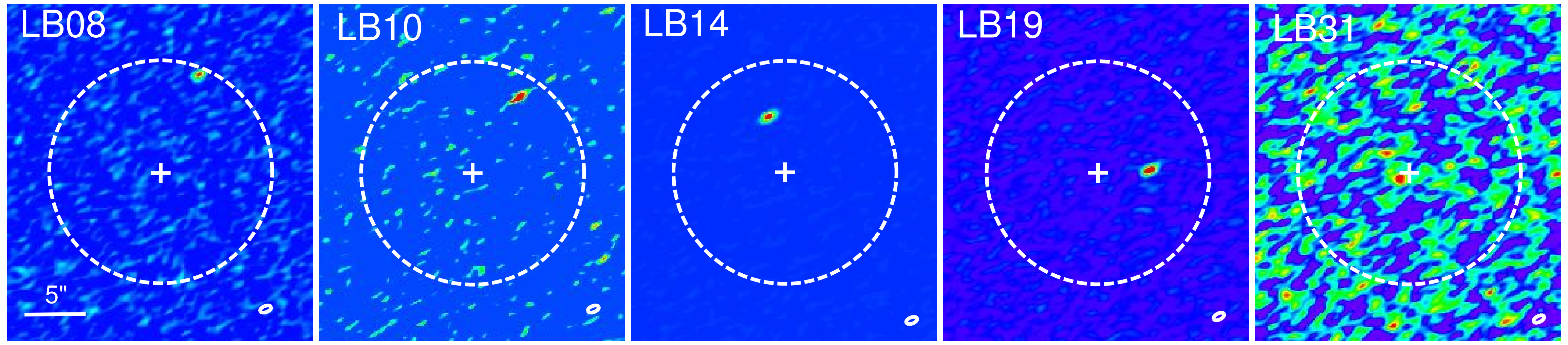

Fig. 2. The five sources detected at 880 μm with ALMA in B30. North is up and east to the left. The ALMA beam size is displayed at the bottom right corner of each image. The white dashed circles represent the ALMA beam (18″ diameter), and are centered at the pointing coordinates (phase centers) for each source.

Table 1. ALMA 880 μm detections in the B30 region.

ALMA detection coordinates RA(J2000) [h m s]	Dec(J2000) [° ′ ″]	Separation from phase center [arcsec]	LABOCA source[a]	S_ν [mJy]	rms [mJy/beam]	Mass (ALMA)** [M_{Jup}]	Mass (LABOCA)[b,**] [M_{Jup}]	Missing flux[c] [%]	A_V[d] [mag]	Tentative nature
05:31:22.97	+12:11:34.7	8.7	B30-LB08	5.70	0.26	9	106	87	2.5	VeLLO/pre-BD
05:31:09.29	+12:11:08.8	6.8	B30-LB10	2.20	0.23	3	46	93	1.2	pre-BD
05:31:19.46	+12:09:15.1	4.5	B30-LB14*	44.0	0.25	67	51	0	2.0	YSO
05:31:27.81	+12:05:30.9	4.2	B30-LB19*	10.7	0.20	16	182	86	2.8	YSO
05:31:15.32	+12:03:38.2	0.6	B30-LB31	0.60	0.13	0.9	82	99	2.4	pre-BD

Notes. (a) LABOCA designation number (see BGH16); (b) From BGH16; (c) Percentage of missing flux between ALMA and LABOCA data; (d) From the 2MASS extinction map; (*) Sources with gas emission detected with ALMA; (**) Derived for a dust temperature of 15 K.

- ALMA観測のボーナスとして広がったCO(3-2)に埋もれたコンパクト成分も検出
- APEX/SABOCAでは 8’ x 4’ (と思う)の領域をマッピング（左図）, 350μm,　7.8”ビームで17個のコアを検出

【ALMA検出と赤外線画像との比較】

緑＋：ALMA検出，黄円：ALMA FOV,
シアン円：APEX beam

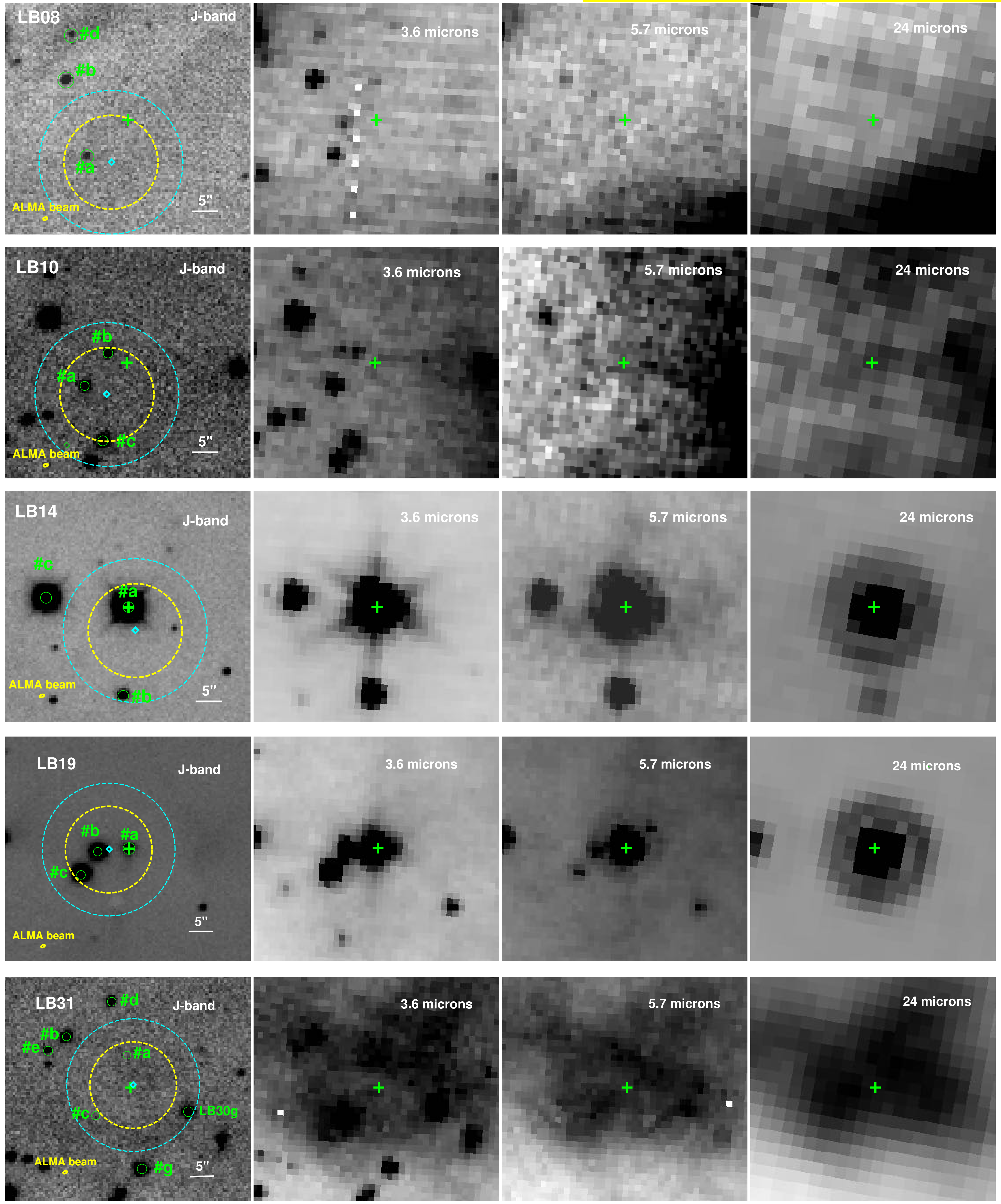

Fig. 4. Infrared (CAHA/O2000 and *Spitzer*/IRAC and MIPS) images centered on the ALMA detection coordinates. North is up and east to the left. We have included in all the *J*-band images (*left panels*) the position of the ALMA detections (green crosses), and the possible infrared counterparts to the APEX/LABOCA detections identified by BGH16 (green labels). The cyan diamonds represent the APEX/LABOCA peak intensity coordinates (ALMA phase center coordinates). We have also plotted the APEX/LABOCA beam of 13.8″ radius (cyan dashed circle), the ALMA FOV of ~18″ diameter (yellow dashed circle), and the ALMA beam at the bottom left corner (yellow solid ellipse).

←対応天体なし（CO検出なし）
APEX/LABOCAで広がっている
(deconvolved size = 27”)

←対応天体なし（CO検出なし）

←対応天体 (Class II)？
星周円盤 (APEXとALMAで同等のFlux)
M = 24-43 M_J (20-30Kを仮定)

←対応天体 (Class I)？
APEX/LABOCAで広がっている
(deconvolved size = 24”)
M(ALMA) ~16 M_J (15Kを仮定)

←対応天体なし（CO検出も）

赤外線の対応天体がないのは，
VeLLOs（低質量原始星）か
Starless Cores（BDのprecursors)？

検出率 5/30，大部分のLABOCA Coreは
6”（2400au）以上に広がった構造

CO(3-2)検出

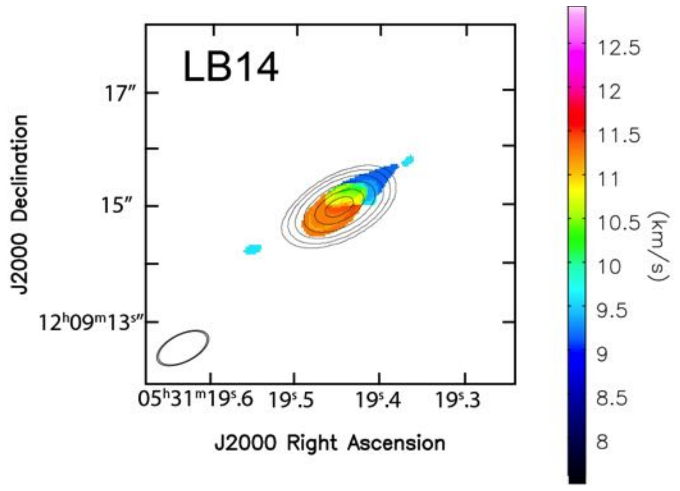

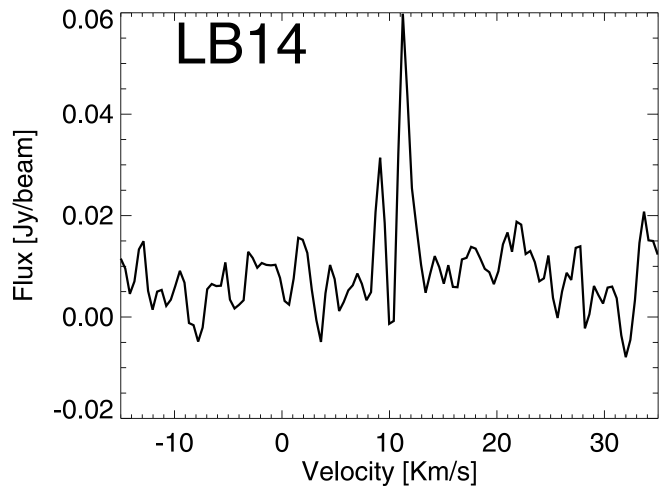

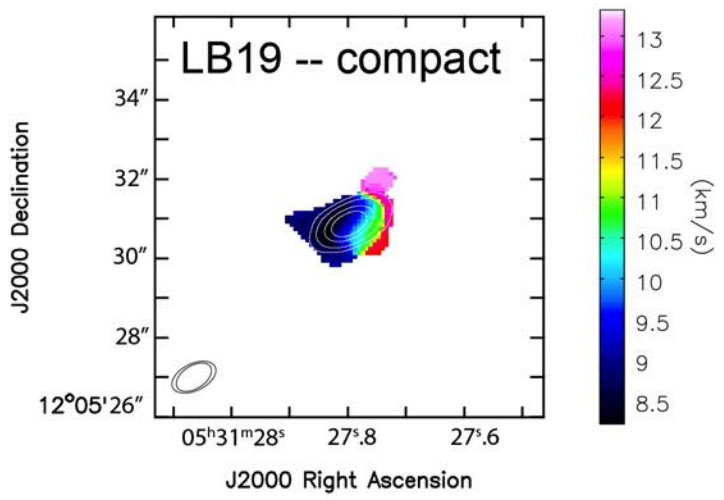

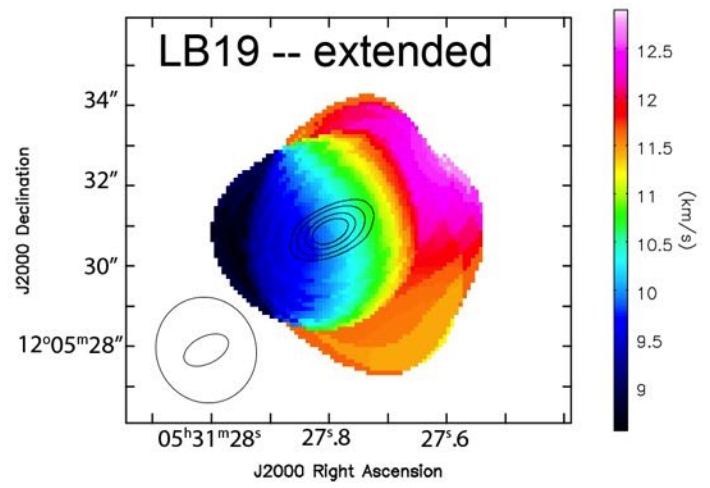

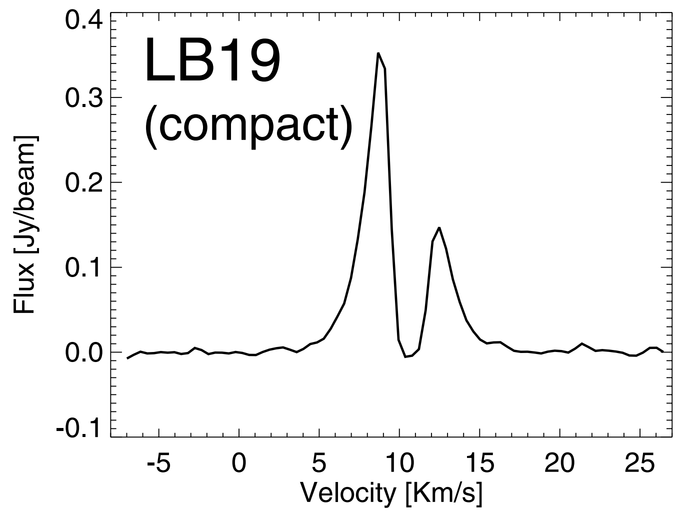

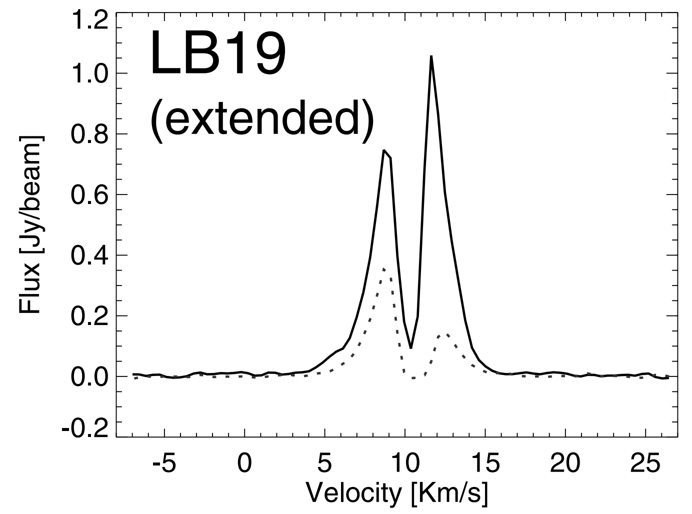

【SABOCA検出（コントア）とIRAC 3.6μm画像，8μm(SB14)との比較】

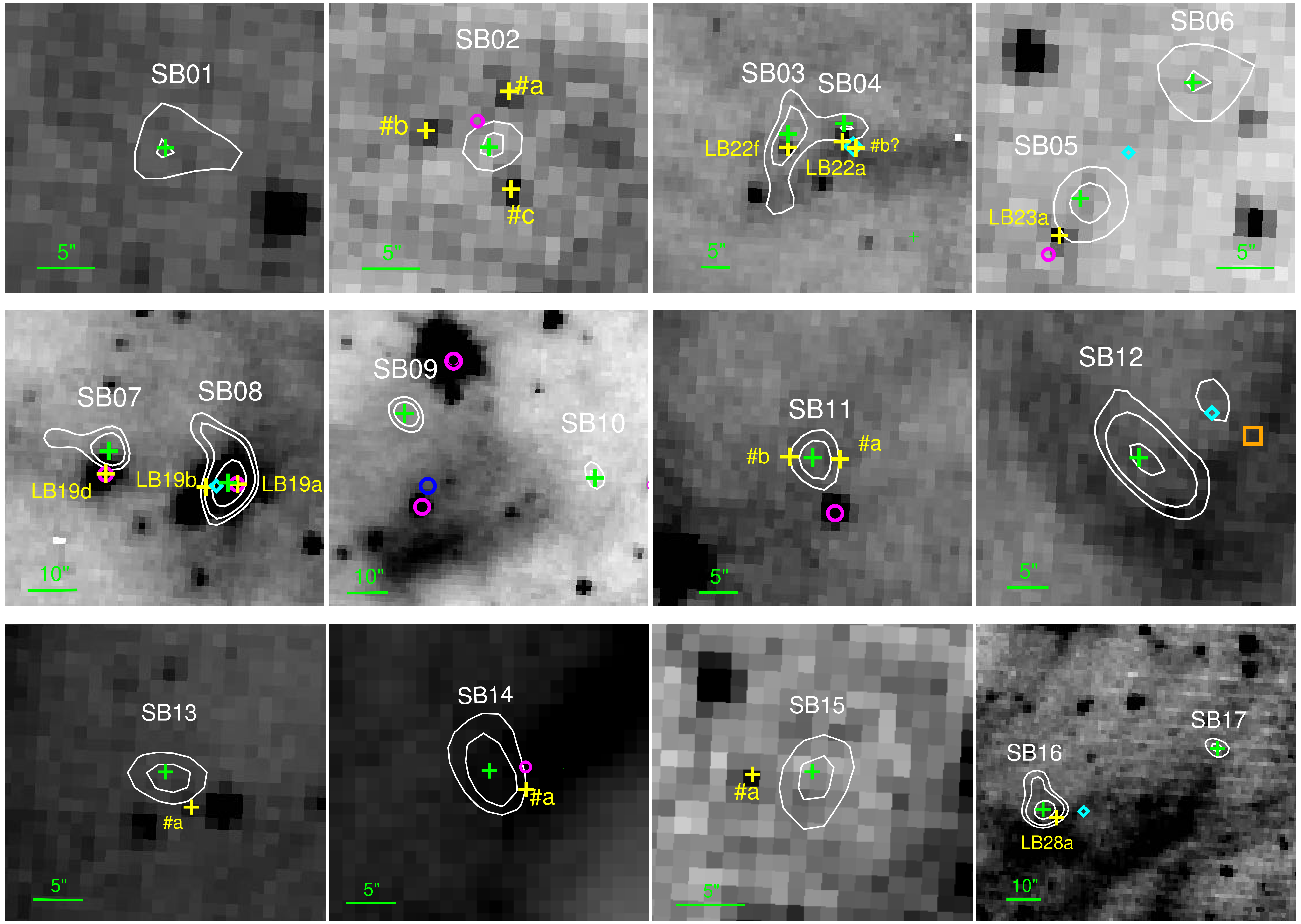

Fig. 8. *Spitzer* IRAC 3.6 μm finding charts with the APEX/SABOCA detections, except for SB14 (IRAC 8 μm image). North is up and east to the left. The green crosses represent the coordinates of the peak emission of the APEX/SABOCA detections. The white contours represent the APEX/SABOCA emission at 2.5, 3, 4 and 5σ level. The infrared counterparts within a radius of $5\farcs3$ (half of the APEX/SABOCA beam) are represented by yellow crosses. If previously discussed by BGH16, they are named with the APEX/LABOCA designation. If not, they are named with low-case letters. The magenta circles represent WISE detections, the cyan diamonds represent the position of the APEX/LABOCA cores peak intensity, and the blue circles indicate *AKARI* detections. The orange square represents a *Planck* detection (see text).

SEDも含めて
個々の天体の性質を
簡単に議論している

19. The ALMA-PILS survey: 3D modeling of the envelope, disks and dust filament of IRAS 16293–2422

S. K. Jacobsen et al. (A&A, in press)

http://ads.nao.ac.jp/abs/2017arXiv171206984J

【内容】PILS(Protostellar Interferometric Line Survey)で観測している Protobinary (IRAS16293-2422) の^{13}CO/C^{17}O/C^{18}O(3-2)データを3D輻射輸送計算で解析 → 星周円盤の構造，それぞれのLuminosityなど議論

3つの主要なトピックス

(i) 2つ中心星がある時の原始星周辺領域の温度構造(特に1Dとの違い)

(ii) I16293 に対するダスト温度構造モデリング(SEDとimageを制限に)

(iii) CO isotoplogues データを使った円盤構造等の議論

Class 0に分類，過去の研究により‥

- d = 120pcを採用
- 16293A : highly active (色々なアウトフロー現象付随)
- 16293B : more quiescent
- separation = 5.3”, or 636 au
- total luminosity = 21±5 L☉

868μm ダスト連続波イメージ

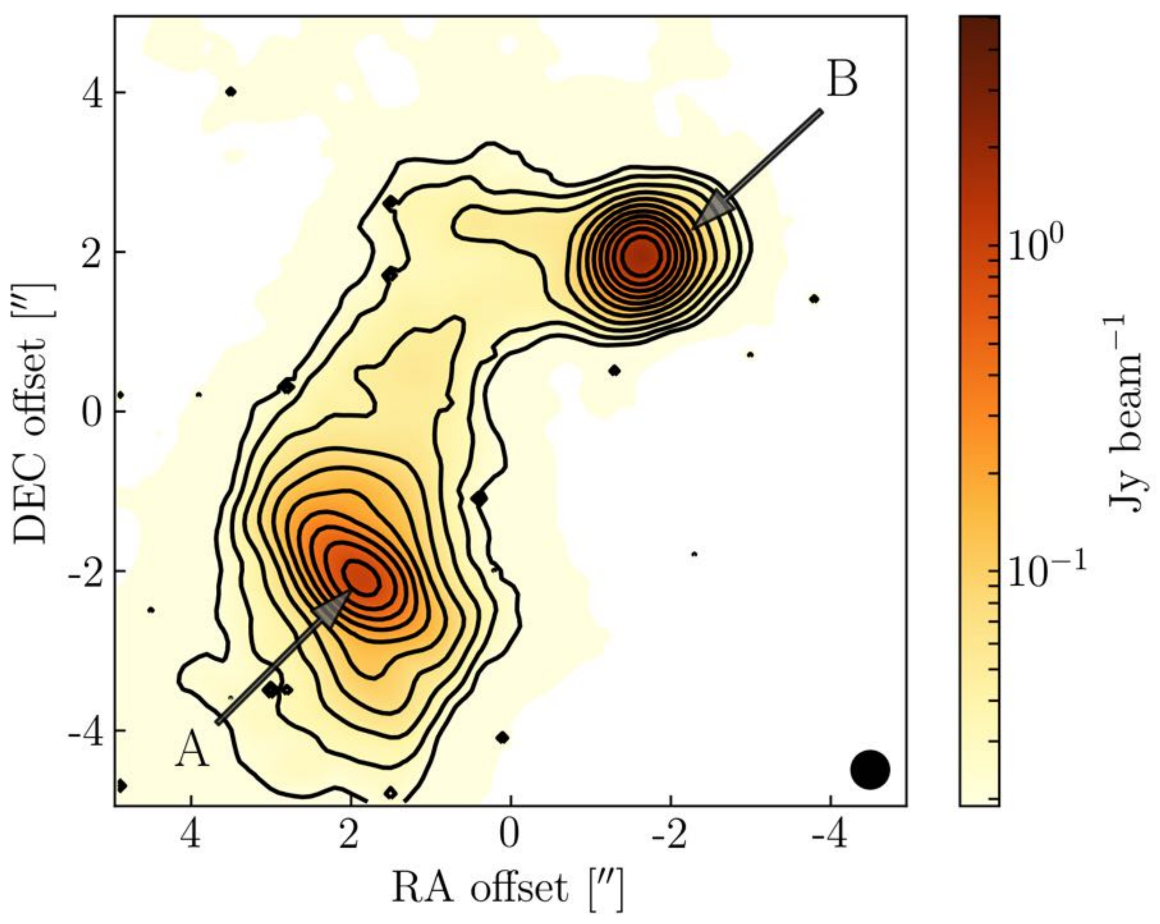

COの積分強度マップ

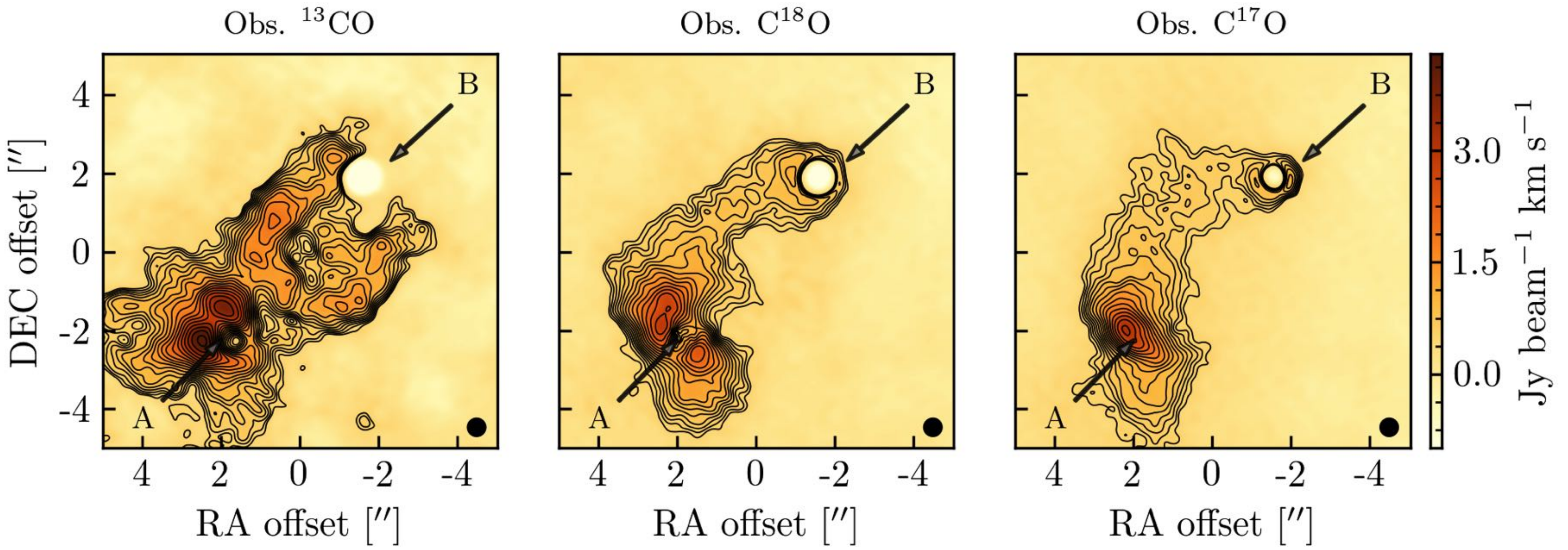

- C^{17}Oがもっともダスト連続波と類似(arc構造)：光学的に薄い
- B方向で強い吸収(ダスト連続波を背景に)

(i) 一般的な設定によるdust 温度分布（詳細次ページ）

- RADMC 3Dを使用，適当なdust modelを仮定 (温度構造を反映)
- エンベロープ + PPDISK 構造，エンベロープは2つのパート

$$\rho(r) = \begin{cases} \rho_0 \left(\frac{r}{r_0}\right)^{-p} & , \text{ if } r \geq r_{\rm plat} \\ \rho_0 \left(\frac{r_{\rm plat}}{r_0}\right)^{-p} & , \text{ if } r < r_{\rm plat}. \end{cases} \quad (1)$$

Power-law, p=1.7

Plateau, r_{plat} = 600au

重要な結果

エンベロープ温度構造（30K, 50K, 90K以上の領域の体積）が輻射源が1つか2つかで大きく変わる（2ページ後）

モデルパラメーター

le 1: `RADMC-3D` model parameters

Parameter	Description	Value
Grid		
r_{out}	Envelope radius	$8{\times}10^{3}$ AU
r_{in}	Grid start radius	5 AU
r_{plat}	Radius of the density plateau	600 AU
n_{θ}	Number of grid cells in the polar range	131
n_{ϕ}	Number of grid cells in the azimuthal range	131
Temperature analysis		
$n_{\mathrm{r,\,out}}$	Number of grid cells in the outer radial region ($r > 600$ AU)	88
$n_{\mathrm{r,\,in}}$	Number of grid cells in the inner radial region ($r \leq 600$ AU)	110
n_{photons}	Number of photons used in thermal Monte Carlo process	$5{\times}10^{7}$
L_{A}	Luminosity of source A	3 – 20 $\mathrm{L}_{\odot}$
One radiation source		
r_{oct}	Octree refinement radius around source	400 AU
$n_{\mathrm{octree\ levels}}$	Octree refinement number	1
Two radiation sources		
r_{oct}	Octree refinement radius around each source	250 AU
$n_{\mathrm{octree\ levels}}$	Octree refinement number	2
IRAS 16293 model		
$n_{\mathrm{r,\,out}}$	Grid cells in the outer radial region ($r > 600$ AU)	22
$n_{\mathrm{r,\,in}}$	Grid cells in the inner radial region ($r \leq 600$ AU)	110
$\rho_{0,\,\mathrm{env}}$	Envelope reference density at $r_{0,\,\mathrm{env}}$	$2.5{\times}10^{-14}$ g cm^{-3}
$r_{0,\,\mathrm{env}}$	Envelope reference radius	1 AU
p_{env}	Envelope density power-law exponent	1.7
M_{A}	Source A stellar mass	1 $\mathrm{M}_{\odot}$
M_{B}	Source B stellar mass	0.1 $\mathrm{M}_{\odot}$
$^{\dagger}T_{\mathrm{eff}}$	Star surface temperature	5000 K
L_{A}	Source A luminosity	3 – 20 $\mathrm{L}_{\odot}$
$r_{0,\,\mathrm{disk}}$	PP-disk reference radius	10 AU
$r_{\mathrm{inner\ disk}}$	Disk inner radius	1 AU
$r_{\mathrm{disk,A}}$	Disk A radius	150 AU
$r_{\mathrm{disk,B}}$	Disk B radius	50 AU
Disk constraints		
$F_{\mathrm{peak,\,A}}$	Peak flux density toward source A	1.0 Jy beam^{-1}
$F_{\mathrm{peak,\,B}}$	Peak flux density toward source B	2.0 Jy beam^{-1}
Disk A aspect ratio	...	1.64
$N_{\mathrm{H_2,\,B}}$	Disk B column density	$\geq 1.2{\times}\,10^{25}$ cm^{-2}
PP-disk models		
Σ_{A}	Parameter space for reference surface density of PP-disk A at 10 AU	0.1 – 5.0 g cm^{-2}
Σ_{B}	Parameter space for reference surface density of PP-disk B at 10 AU	1.0 – 12.0 g cm^{-2}
Ψ	Parameter space of the PP-disks flaring constants	0 – 0.25
p	Parameter space of the PP-disks dust density radial power-law exponents	0.5 – 1.5
$H_{0,\mathrm{A}}$	Parameter space of PP-disk A scale-height at 10 AU	0.85 – 2.0 AU
$H_{0,\mathrm{B}}$	Parameter space of PP-disk B scale-height at 10 AU	0.85 – 3.0 AU
i_{A}	Parameter space of PP-disk A inclination, 90° is edge-on	30 – 90°
$n_{\mathrm{lev,\,disk}}$	Octree refinement level of entire disk	2
$n_{\mathrm{lev,\,in\ disk}}$	Octree refinement level in innermost region	4
n_{photons}	Number of photons used in thermal Monte Carlo process	10^{7}
Rotating toroid models		
$r_{c,\,\mathrm{A}}$	Parameter space of the centrifugal radius of rotating toroid A	50 – 100 AU
$r_{c,\,\mathrm{B}}$	Parameter space of the centrifugal radius of rotating toroid A	5 – 40 AU
$\dot{M}_{\mathrm{A}}$	Parameter space of the mass accretion rate into source A	$1.0{\times}10^{-6}$ – $5.5{\times}10^{-6}$ $\mathrm{M}_{\odot}$ yr^{-1}
$\dot{M}_{\mathrm{B}}$	Parameter space of the mass accretion rate into source B	$1.0{\times}10^{-6}$ – $5.5{\times}10^{-6}$ $\mathrm{M}_{\odot}$ yr^{-1}
$n_{\mathrm{lev,\,disk}}$	Octree refinement level of entire disk	2
$n_{\mathrm{lev,\,in\ disk}}$	Octree refinement level in innermost region	2
n_{photons}	Number of photons used in thermal Monte Carlo process	10^{6}
Dust arc		
ρ_{0}	Reference density	$2.5\,{\times}10^{-17}$ g cm^{-3}
r_{out}	Filament radius from filament center	130 AU
Filament semi-minor axis	...	170 AU
Filament semi-major axis	...	300 AU

Notes. Model parameters for each setup. L_{B} is always defined as $L_{\mathrm{B}} = 21.0\ \mathrm{L}_{\odot}$ - L_{A}. †The radiation spectra of both source A and B are treate blackbodies with a temperature of 5000 K, following Schöier et al. (2002).

連星系と単独星の
ある温度以上の領域の
相対的な差

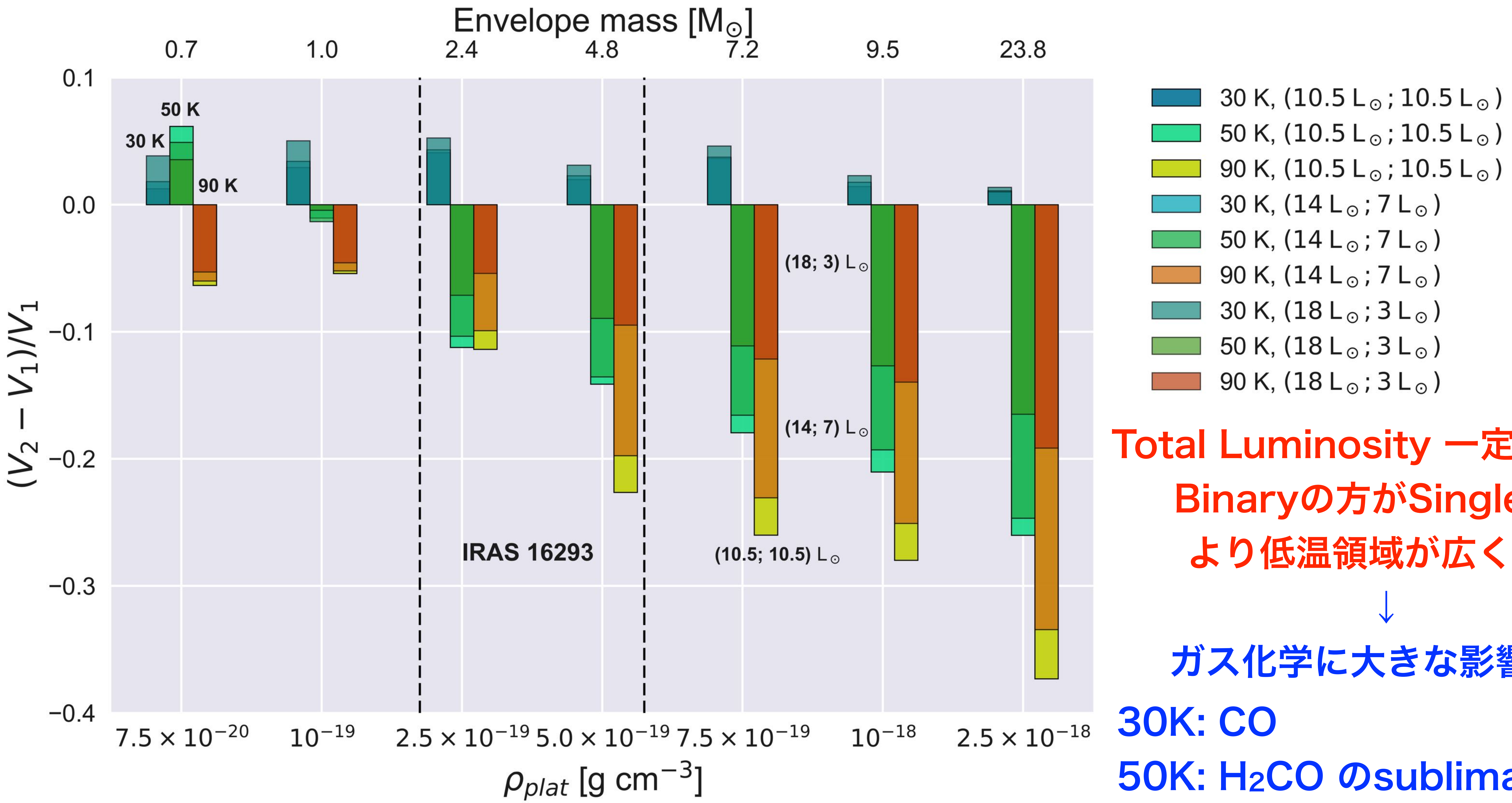

Total Luminosity 一定の下では
Binaryの方がSingleより
より低温領域が広くなる
↓
ガス化学に大きな影響あり

30K: CO
50K: H_2CO のsublimation T.
90K; H_2O

低い <―― 中心密度 ――> 高い

Fig. 3: Relative differences in volumes of dust above different temperatures. The volume difference between the single star temperature volume, V_1, and binary star temperature volume, V_2, is shown, normalized to V_1, i.e. $\tau - 0.2$ means that the total temperature volume is 20 % lower if there are two stars compared to one. The envelope mass range is 0.7 – 24 $M_\odot$, consistent with the dense core mass range observed in (Alves et al. 2007). The relevant mass range for IRAS 16293 is 2.4 – 4.8 $M_\odot$, (our IRAS 16293 envelope model has a mass of ~4 $M_\odot$). There is a clear tendency for a single star to result in more dust heated above ~ 50 K.

(ii) Dust 放射モデリング

・M_A = 1.0$M_\odot$, $M_B \leq 0.1 M_\odot$ （過去の速度場の解析から）, r_{plat}の内側にdiskコンポーネント, ２つのダスト密度モデル（半径は150au, 50auで固定）

・静水圧平衡で記述されるPPDisk=DM。Bはface on仮定, Aの傾き角はfree parameter, イメージに加えSEDも制約として使う

・回転トロイドモデル”rotating toroid model” = RTM (Hartmann 2009: 元はHartmann, Calvet, Boss 1996)：角運動量保存で落下する流線の無限遠方で, シート形状平衡解の重みをつけた密度モデル

$$\rho(r,\theta) = \frac{\dot{M}\left(1+\frac{\cos\theta}{\cos\theta_0}\right)^{-1/2}}{4\pi\sqrt{GM_* r^3}}\left(\frac{\cos\theta}{\cos\theta_0}+\frac{2\cos^2\theta_0}{r/r_c}\right)^{-1},$$

r_c: centrifugal radius

・arc構造については柱密度一定の形で入れる

DMに比べて RTMは鉛直方向に 広がり, 赤道面へのoptical depthが小さくなり, dust温度高い

Table 2: Example dust model parameters.

PP-disk model	L_A [$L_\odot$]	L_B [$L_\odot$]	$\Sigma_{0,A}$ [g cm^{-2}]	$\Sigma_{0,B}$ [g cm^{-2}]	$H_{0,A}$ [AU]	$H_{0,B}$ [AU]	i_A [°]
DM 1	18.0	3.0	1.0	3.0	1.25	1.5	55
DM 2	14.0	7.0	1.0	0.05	0.85	2.0	50
DM 3	10.5	10.5	1.0	0.05	1.25	2.0	60
Rotating toroid model	L_A [$L_\odot$]	L_B [$L_\odot$]	$\dot{M}_A$ [$M_\odot$ yr^{-1}]	$\dot{M}_B$ [$M_\odot$ yr^{-1}]	$r_{c,A}$ [AU]	$r_{c,B}$ [AU]	
RTM 1	18.0	3.0	3.75×10^{-6}	2.75×10^{-6}	75	20	
RTM 2	10.5	10.5	2.1×10^{-6}	2.1×10^{-6}	50	20	
RTM 3	20.0	1.0	3.8×10^{-6}	4.6×10^{-6}	75	20	
RTM 4	7.0	14.0	3.0×10^{-6}	2.0×10^{-6}	75	20	
RTM 5	3.0	18.0	3.0×10^{-6}	2.0×10^{-6}	75	20	

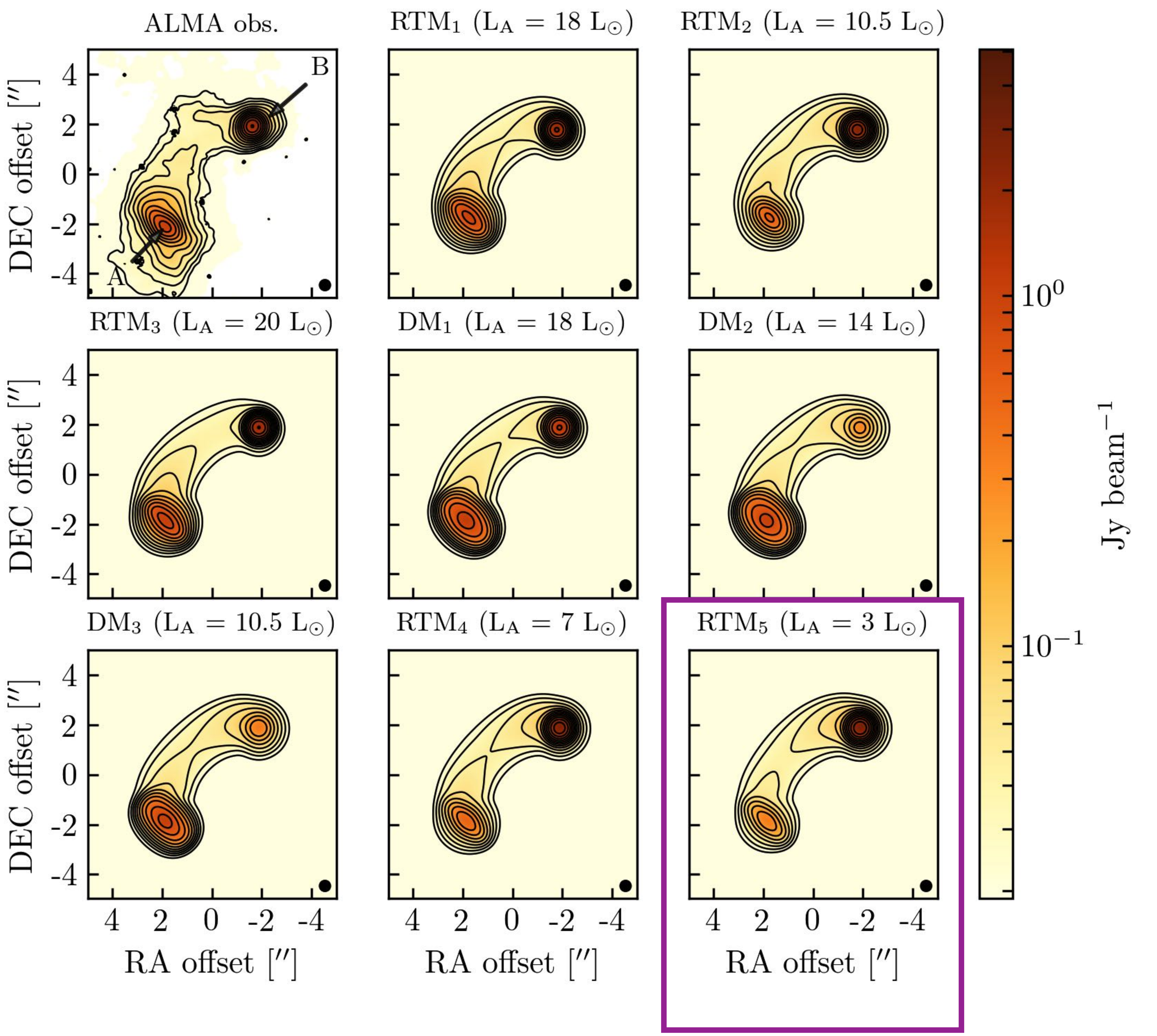

２つのダストピークの値を合わせることは どのモデルでもある程度可能

(iii) CO 放射モデリング

・LIMEを使って計算，g/d=100とする
・non-LTE，ただしガス温度=ダスト温度は仮定
・DMの場合はケプラー回転，RTMの場合は回転自由落下(Tereby, Shu, Cassen 1984)
・CO isotopologues アバンダンス比を振った例もappendixにはあり

Table 3: LIME model parameters

Parameter	Description	Value
Grid outer radius	…	2×10^3 AU
Grid start radius	…	30 AU
n_{nodes}	Number of grid nodes in the LIME calculations	7×10^4
CO/H_2	Standard ISM abundance of CO	10^{-4}
$^{13}CO/H_2$	Standard ISM abundance of ^{13}CO	1.30×10^{-6}
$C^{18}O/H_2$	Standard ISM abundance of $C^{18}O$	1.79×10^{-7}
$C^{17}O/H_2$	Standard ISM abundance of $C^{17}O$	5.58×10^{-8}
Freeze out factor	…	0.01
Gas-to-dust-mass ratio	Used for all conversions from dust to gas mass	100
CO isotopologues abundances of all models		
$X_{^{13}CO}$	^{13}CO abundance	2.6×10^{-7}
$X_{C^{18}O}$	$C^{18}O$ abundance	3.58×10^{-8}
$X_{C^{17}O}$	$C^{17}O$ abundance	1.12×10^{-8}

Parameter	Description	Value
Rotating toroid model		
L_A	Luminosity of source A	18 $L_\odot$
L_B	Luminosity of source B	3 $L_\odot$
$\dot{M}_A$	Mass accretion rate	3.75×10^{-6} $M_\odot$ yr^{-1}
$\dot{M}_B$	Mass accretion rate	2.75×10^{-6} $M_\odot$ yr^{-1}
$r_{c,A}$	Centrifugal radius	75 AU
$r_{c,B}$	Centrifugal radius	20 AU
PP-disk model		
L_A	Luminosity of source A	14 $L_\odot$
L_B	Luminosity of source B	7 $L_\odot$
$\Sigma_{0,A}$	Dust surface density at 10 AU	0.6 g cm^{-2}
$\Sigma_{0,B}$	Dust surface density at 10 AU	5.0 g cm^{-2}
$H_{0,A}$	Scale-height at 10 AU	1.5 AU
$H_{0,B}$	Scale-height at 10 AU	2.0 AU
i_A	Disk A inclination	60°

RTMの方が
Aの「放射」をよく再現
「スケールハイトが大きい必要あり」

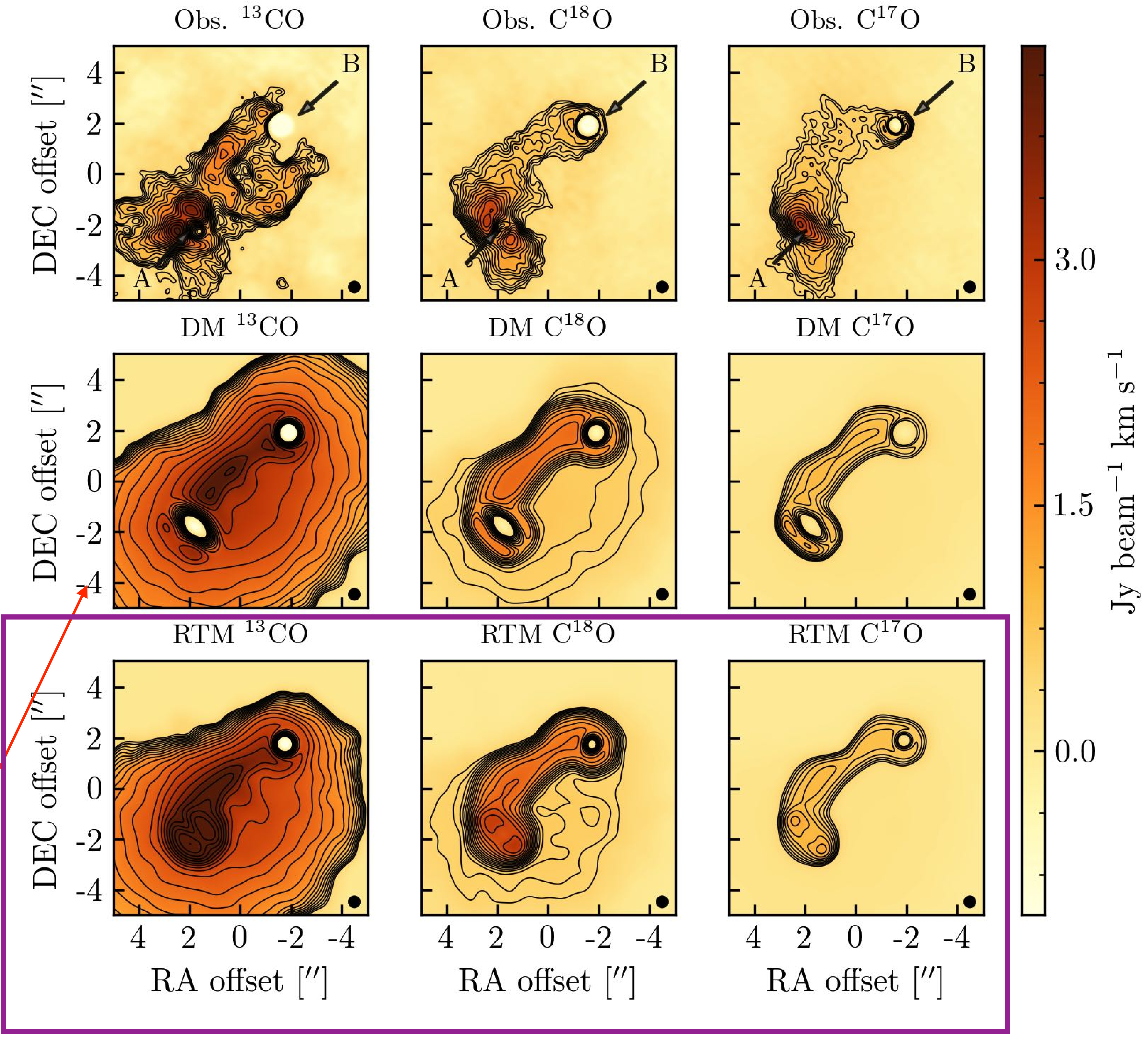

RTM

DM

Hが小さいと
吸収しすぎ

RTM（ダストピークを再現する）の場合でLuminosity比を変えた場合の
$C^{17}O$シミュレーション，$L_A \gtrsim 18 L_\odot$ 必要

Table 5: LIME model parameters of Fig. 6.

Model	$\dot{M}_A$ [$M_\odot$ yr^{-1}]	$\dot{M}_B$ [$M_\odot$ yr^{-1}]
L_A = 3 $L_\odot$	9.0×10^{-6}	1.3×10^{-6}
L_A = 7 $L_\odot$	5.5×10^{-6}	1.4×10^{-6}
L_A = 10.5 $L_\odot$	4.6×10^{-6}	1.6×10^{-6}
L_A = 14 $L_\odot$	4.2×10^{-6}	1.85×10^{-6}
L_A = 18 $L_\odot$	3.75×10^{-6}	2.75×10^{-6}
L_A = 20 $L_\odot$	3.8×10^{-6}	4.6×10^{-6}

Notes. All models are rotating toroids, using $r_{c,A}$ = 75 AU and $r_{c,B}$ = 20 AU.

が
まあまあ
あっているかなという
モデル（CO，dustとも）

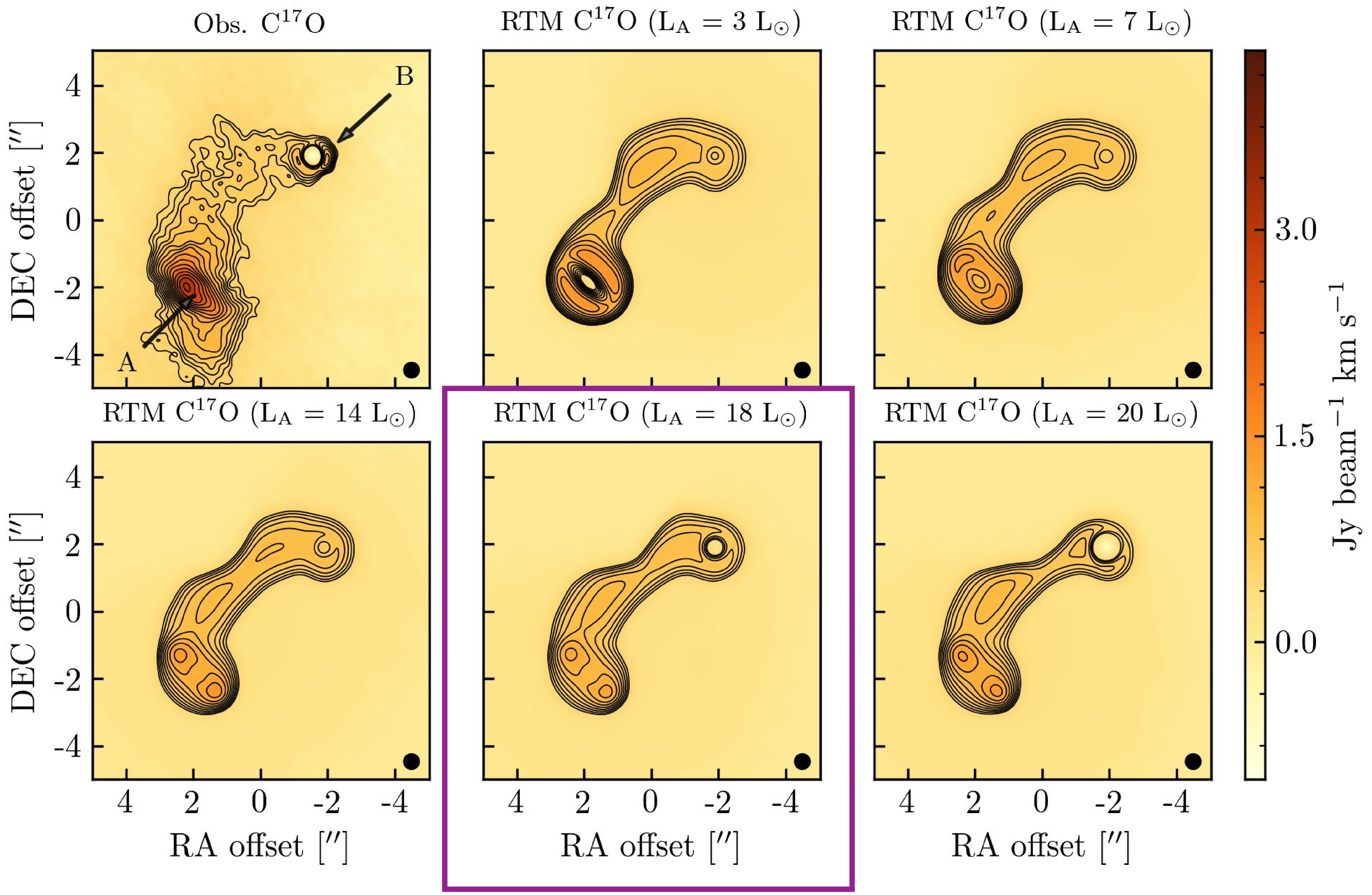

Fig. 6: Observed and modeled $C^{17}O$ zeroth moment maps, contour levels are divided logarithmically from 0.5 to 7.3 Jy beam^{-1} km s^{-1}. All models are rotating toroid models matching the dust continuum peak flux densities for disk A and B.

DMでBの吸収を合わせようとすると，
極端に大きなHが必要 H > 3.0au @ r=10au（原始星ではよくある）

History of Globulettes in the Milky Way

Tiia Grenman[1], Erik Elfgren[1] and Hans Weber[1]

[1] Luleå University of Technology, Sweden

E-mail contact: tiia.grenman *at* ltu.se

Globulettes are small (radii $<$ 10 kAU) dark dust clouds, seen against the background of bright nebulae. A majority of the objects have planetary mass. These objects may be a source of brown dwarfs and free floating planetary mass objects in the galaxy. In this paper we investigate how many globulettes could have formed in the Milky Way and how they could contribute to the total population of free floating planets. In order to do that we examine H-alpha images of 27 H II regions. In these images, we find 778 globulettes.
We find that a conservative value of the number of globulettes formed is 5.7×10^{10}. If 10 % of the globulettes form free floating planets then they have contributed with 5.7×10^{9} free floating planets in the Milky Way. A less conservative number of globulettes would mean that the globulettes could contribute 2.0×10^{10} free floating planets. Thus the globulettes could represent a non-negligible source of free floating planets in the Milky Way.

Accepted by Astrophysics and Space Science

http://urn.kb.se/resolve?urn=urn:nbn:se:ltu:diva-67161
http://arxiv.org/pdf/1801.01355

HII領域の画像を丹念に調べて，Globulettes のサイズ分布や銀河系内の総数を見積もり。
フリーフローティングプラネットの起源（母胎）か？
画像があれば良かったのだが。。。

Detection of a centrifugal magnetosphere in one of the most massive stars in the ρ Oph star-forming cloud

S. Hubrig[1], M. Schöller[2], S. P. Järvinen[1], M. Küker[1], A. F. Kholtygin[3] and P. Steinbrunner[4]

[1] AIP, Germany, [2] ESO, Germany, [3] Saint-Petersburg State University, Russia, [4] FU Berlin, Germany

E-mail contact: shubrig *at* aip.de

Recent XMM-Newton observations of the B2 type star ρ Oph A indicated a periodicity of 1.205 d, which was ascribed to rotational modulation. Since variability of X-ray emission in massive stars is frequently the signature of a magnetic field, we investigated whether the presence of a magnetic field can indeed be invoked to explain the observed X-ray peculiarity. Two FORS 2 spectropolarimetric observations in different rotation phases revealed the presence of a negative ($\langle B_z\rangle_{\rm all} = -419 \pm 101$ G) and positive ($\langle B_z\rangle_{\rm all} = 538 \pm 69$ G) longitudinal magnetic field, respectively. We estimate a lower limit for the dipole strength as $B_{\rm d} = 1.9 \pm 0.2$ kG. Our calculations of the Kepler and Alfvén radii imply the presence of a centrifugally supported, magnetically confined plasma around ρ Oph A. The study of the spectral variability indicates a behaviour similar to that observed in typical magnetic early-type Bp stars.

Accepted by AN

https://arxiv.org/pdf/1712.05939

X線変光から1.2日で自転しているらしいことがわかった ρOph A中の B2型星のZeeman観測による磁場調査。異なる自転フェーズ角の測定から，磁場強度やDipole成分を見積もり。

20

First Results from the *Herschel* and ALMA Spectroscopic Surveys of the SMC: The Relationship Between [C II]-bright Gas and CO-bright Gas at Low Metallicity

Katherine E. Jameson[1,2], Alberto D. Bolatto[1], Mark Wolfire[1], Steven R. Warren[3], Rodrigo Herrera-Camus[4], Kevin Croxall[5,6], Eric Pellegrini[7], John-David Smith[8], Monica Rubio[9], Remy Indebetouw[10,11], Frank P. Israel[12], Margaret Meixner[13], Julia Roman-Duval[13], Jacco Th. van Loon[14], Erik Muller[15], Celia Verdugo[16], Hans Zinnecker[17] and Yoko Okada[18]

The Small Magellanic Cloud (SMC) provides the only laboratory to study the structure of molecular gas at high resolution and low metallicity. We present results from the *Herschel* Spectroscopic Survey of the SMC (HS^3), which mapped the key far-IR cooling lines [C II], [O I], [N II], and [O III] in five star-forming regions, and new ALMA 7m-array maps of ^{12}CO and ^{13}CO $(2-1)$ with coverage overlapping four of the five HS^3 regions. We detect [C II] and [O I] throughout all of the regions mapped. The data allow us to compare the structure of the molecular clouds and surrounding photodissociation regions using ^{13}CO, ^{12}CO, [C II], and [O I] emission at $\lesssim$10 *arcsec* (< 3 pc) scales. We estimate A_V using far-IR thermal continuum emission from dust and find the CO/CII ratios reach the Milky Way value at high A_V in the centers of the clouds and fall to $\sim 1/5 - 1/10\times$ the Milky Way value in the outskirts, indicating the presence of translucent molecular gas not traced by bright ^{12}CO emission. We estimate the amount of molecular gas traced by bright [C II] emission at low A_V and bright ^{12}CO emission at high A_V. We find that most of the molecular gas is at low A_V and traced by bright [C II] emission, but that faint ^{12}CO emission appears to extend to where we estimate the H_2-to-HI transition occurs. By converting our H_2 gas estimates to a CO-to-H_2 conversion factor (X_{CO}), we show that X_{CO} is primarily a function of A_V, consistent with simulations and models of low metallicity molecular clouds.

Accepted by ApJ

Low-metal環境であるSMCに含まれている星間物質（分子雲成分）を対象に遠赤外禁制線[CII], [OI], [NII], [OIII]（Herschel）とCO (ALMA/ACA)を組み合わせて解析。分子雲のLow Av領域はCOが解離していて放射は見えず，[CII]でトレースされている。

Dynamics of magnetic flux tubes and IR-variability of Young Stellar Objects

Sergey Khaibrakhmanov[1,2], Alexander Dudorov[2], Andrey Sobolev[1]

[1] Kourovka astronomical observatory, Ural Federal University, Ekaterinburg 620000, Russia
[2] Theoretical physics department, Chelyabinsk state university, Chelyabinsk 454001, Russia

E-mail contact: khaibrakhmanov *at* csu.ru

We simulate the dynamics of slender magnetic flux tubes (MFTs) in the accretion disks of T Tauri stars. The dynamical equations of our model take into account the aerodynamic and turbulent drag forces, and the radiative heat exchange between the MFT and ambient gas. The structure of the disk is calculated with the help of our MHD model of the accretion disks. We consider the MFTs formed at the distances 0.027–0.8 au from the star with various initial radii and plasma betas β_0. The simulations show that the MFT with weak magnetic field ($\beta_0 = 10$) rise slowly with speeds less than the sound speed. The MFTs with $\beta_0 = 1$ form outflowing magnetized corona of the disk. Strongly magnetized MFTs ($\beta_0 = 0.1$) can cause the outflows with velocities 20–50 km s^{-1}. The tubes rise periodically over times from several days to several months according to our simulations. We propose that periodically rising MFTs can absorb stellar radiation and contribute to the IR-variability of Young Stellar Objects.

Accepted by RAA

http://arxiv.org/pdf/1712.09094

円盤内縁部の理論的構造解析に基づき，YSOsが示す赤外変光と関連させて議論。